Dielectric-Modulated Bulk-Planar Junctionless Field-Effect Transistor for Biosensing Applications

Deepika Singh and Ganesh C. Patil

***Abstract*— In this article, we have focused on the concept of junction-free transistor to propose and simulate the ultrathin dielectric modulated (DM) bulk-planar junctionless field-effect transistor (BP-JLFET) as a biosensor device. The proposed device is incorporated with a label-free detection of neutral (proteins, enzymes, streptavidin, and APTES) and charged [deoxyribonucleic acid (DNA)] biomolecules in terms of dielectric constant (K) and charge densities (ρ). For the detection of the biomolecules, the nanocavity is formed by etching out the oxide underneath the gate dielectric at source end. The presence/absence of biomolecules has been detected by the factor of sensitivity with the immobilization of dielectric constant (K) and the charge density (ρ) in the formed nanocavity. Moreover, the comparative study of the BP-JLFET, the dielectric-modulated tunnel field-effect transistor (DM-TFET), and the conventional dielectric-modulated field-effect transistor (DM-FET)-based biosensor in terms of their drain current (I_{ds}) and the sensitivity have been carried out. From the study, it can be depicted that the BP-JLFET has higher sensitivity to sense the biomolecules compared to both the DM-TFET and the conventional DM-FET. Furthermore, we have also analyzed the noise characteristics for the simulated structures to measure the ability of the proposed device for sensing the biomolecules in the presence of noise.**

***Index Terms*— Biosensor, bulk planar, junctionless, nanocavity, sensitivity.**

I. Introduction

IN TODAY'S era, the point-of medical healthcare becomes one of the major factors among the aging population. For this, several biosensors have been researched to detect the presence of various diseases in the human body, such as blood glucose, diabetes, and early age detection of cancer. Among various nanotechnology-based biosensors, the ion-sensitive field-effect transistor (ISFET) has attracted many researchers due to its high capability of sensing the presence of charged biomolecules [1]. As from the study [2], [3], these biosensors are incapable for detection of neutrally charged biomolecules. Therefore, a dielectric-modulated field-effect transistor (DM-FET)-based biosensor became popular for its potentiality to detect both charged and neutral charged biomolecules with higher sensitivity [4], [5], [6]–[8]. These biosensors have various advantages in terms of low-cost label-free detection, miniaturization, and better response with higher sensitivity. The working principle of FET and DM-FET is the same beside the formation of nanocavity underneath the gate dielectric of the DM-FET-based structure to detect the various biomolecules [9], [10]. For the detection of neutral (proteins, enzymes, streptavidin, and APTES) and charged [deoxyribonucleic acid (DNA)] biomolecules, the dielectric constant and the charge density are considered as the electrical parameters, which varies the electrical characteristics by the immobilization of the biomolecules in the nanocavity. The variations occurred in the electrical characteristics have been used to evaluate the sensitivity, which results in detection of biomolecules in the nanocavity of the device. In addition to these, the FET-based biosensors face some limitations during the fabrication process, such as short-channel effects and random dopant fluctuations [11], [12]. To create source and drain regions, physical doping is used. This leads to the complexity in fabrication of device with higher thermal budget [11]. Apart from this, the abrupt junction profile formation also becomes difficult due to the diffusion of carriers from source/drain to channel region [3]. Thus, to solve the aforementioned issues, the junctionless-based device has been introduced, which has numerous advantages in terms of less complexity in the fabrication process and low thermal budget, and it also provides better scalability [2], [3], [13]–[15].

Furthermore, the junctionless transistor (JLT)-based biosensors have been investigated [2], [16]–[17]. In the reported literature [16], the junctionless FET-based biosensor faces the limitation of low sensitivity due to less change in the drain current for the immobilization of different biomolecules. To overcome the limitations of the junctionless FET-based biosensor, double-gate junctionless DM-TFET-based biosensors have been introduced with better sensitivity [2], [17]. However, the double-gate junctionless TFET-based biosensors face more complexity in the fabrication process, which leads to increase in the cost of the device [16].

Therefore, to overcome the above mentioned limitations, we have proposed the bulk-planar junctionless field-effect transistor (BP-JLFET) for biosensing applications. Although the

Manuscript received February 26, 2021; accepted May 19, 2021. Date of publication June 4, 2021; date of current version June 23, 2021. The review of this article was arranged by Editor W. S. Kim. *(Corresponding author: Deepika Singh.)*

The authors are with the Center for VLSI and Nanotechnology, Visvesvaraya National Institute of Technology, Nagpur 440010, India (e-mail: singh.dipikaa999@gmail.com; ganeshcpatil@cvn.vnit.ac.in).

Color versions of one or more figures in this article are available at https://doi.org/10.1109/TED.2021.3083212.

Digital Object Identifier 10.1109/TED.2021.3083212

0018-9383 © 2021 IEEE. Personal use is permitted, but republication/redistribution requires IEEE permission.
See https://www.ieee.org/publications/rights/index.html for more information.

Authorized licensed use limited to: PRABIN KUMAR BERA. Downloaded on September 21,2022 at 13:31:50 UTC from IEEE Xplore. Restrictions apply.

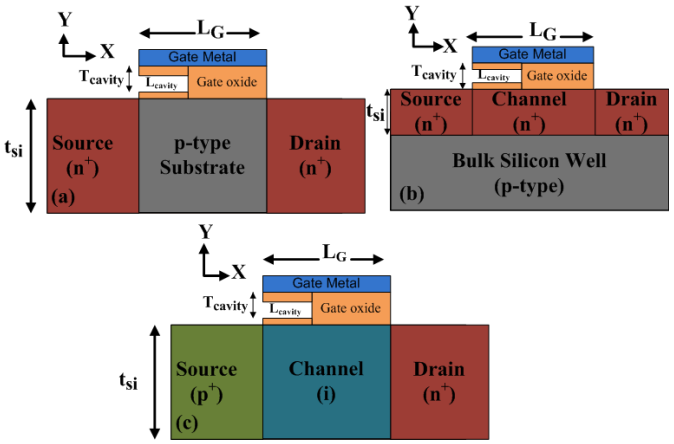

Fig. 1. 2-D cross-sectional view of (a) conventional DM-FET-based biosensor, (b) BP-JLFET-based biosensor, and (c) DM-TFET-based biosensor.

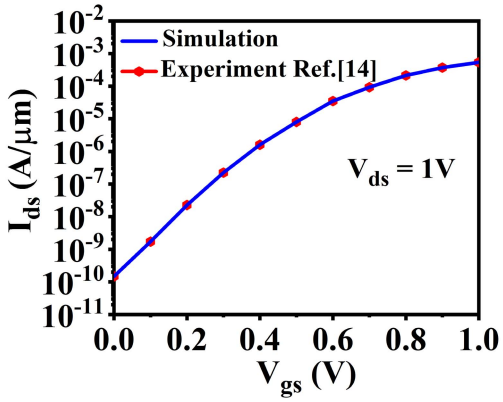

Fig. 2. Plot of transfer characteristics of simulated and experimented n-BPJLFET [14].

proposed BP-JLFET-based biosensor carries source–channel–drain-free junction, it has a junction for isolation in the vertical direction. Furthermore, the fabrication process of the proposed device includes less complex process steps that require low thermal budget [15]. The proposed biosensor also includes the nanocavity to detect the presence of both neutral and charged biomolecules in terms of sensitivity of the device. The nanocavity is formed by etching out the oxide region underneath the gate dielectric of the proposed structure. The dielectric constant and negative charge density have been considered to detect the presence of neutral biomolecules (such as streptavidin, proteins, enzymes, and APTES) and charged biomolecules (DNA) in the nanocavity. The DNA contains negative charges due to the presence of phosphate particles in it. Since the negative charge density is noticeable, it shows the capability to detect the presence of DNA molecules in the formed cavity [18], [19]. Therefore, the proposed device has been analyzed with the variation in electrical characteristics for the immobilization of the neutral and charged biomolecules in the nanocavity. For the proper study, the comparison of the proposed BP-JLFET, the conventional DM-FET, and the DM-TFET-based biosensor has been performed in terms of their sensitivity. The noise characteristics of the conventional DM-FET, BP-JLFET, and the DM-TFET have also been evaluated by considering the linearity parameters.

II. Device Structure, Simulation, and Operation

The 2-D cross-sectional views of the n-channel of the conventional DM-FET, BP-JLFET, and the DM-TFET-based biosensor are shown in Fig. 1(a)–(c), respectively. From Fig. 1(b), it can be seen that the proposed BP-JLFET-based biosensor, n^+-type device layer, is formed on p-type silicon substrate having the concentration of 5×10^{19} cm^{-3}. For the comparison, the conventional DM-FET and the DM-TFET-based biosensor structures have been considered in which the n^+-p-n^+ and p^+-i-n^+ doping are used, respectively, to form the architecture [see Fig. 1(a) and (c)]. The BP-JLFET device incorporates uniform lateral doping to create the source, channel, and drain region, which results in the same doping concentration in the device layer. In the structure of BP-JLFET, the gate metal is formed on upper part of the n-type layer with p-type work function of 5.1 eV. Moreover, all the three structures include the nanocavity underneath the gate dielectric at source end to detect the biomolecules. This nanocavity is formed in all the three structures by etching out the gate dielectric using the wet etching process [7].

The other parameters to design the device are: channel length (L_G) = 40 nm, source length (L_S) = 30 nm, drain length (L_D) = 30 nm, length of cavity (L_{cavity}) = 17 nm, thickness of cavity (T_{cavity}) = 6 nm, device layer thickness (t_{si}) = 10 nm, and thickness of oxide (t_{ox}) = 7 nm for the conventional DM-FET, BP-JLFET, and the DM-TFET. For the simulation of the results, the models used for all the three structures are: Lombardi mobility model and Philips unified mobility model. Shockley–Read–Hall (SRH) and Auger recombination models are used for the recombination of charge carriers. In addition to these, bandgap narrowing and Fermi–Dirac statistics are also incorporated. Apart from these, a nonlocal band-to-band tunneling (BTBT) is used for the consideration of lateral tunneling in BP-JLFET and DM-TFET structures, which occurs between the channel and the drain region of the device. The model parameters used for the evaluation of electrical characteristics of BP-JLFET-based biosensor are matched with the experimental results in [14] (see in Fig. 2).

In this article, the BP-JLFET-based biosensor has been compared with the conventional DM-FET- and DM-TFET-based biosensor to find out the capability of the proposed device for the detection of biomolecules with the higher sensitivity. To detect the neutral and charged biomolecules, the cavities are filled in terms of dielectric constant (K) and negative charge density (ρ), respectively. As the cavity is filled with different dielectric constants (K > 1) and negative charge density in the range of 10^{11}–10^{12} cm^{-2}, the change in transfer characteristics can be noticed, which leads toward the change in the sensitivity of a device. For the measurement of the sensitivity, the change in drain current is measured in terms of the presence and absence of biomolecules in the formed nanocavity. For most of the devices, the sensitivity is also

Authorized licensed use limited to: PRABIN KUMAR BERA. Downloaded on September 21,2022 at 13:31:50 UTC from IEEE Xplore. Restrictions apply.

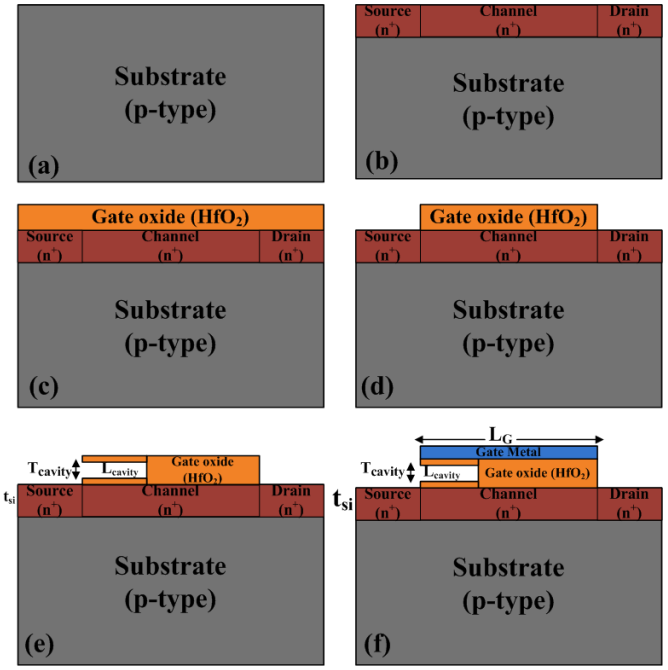

Fig. 3. (a)–(f) Process flow for the fabrication of BP-JLFET-based biosensor.

dependent on the ON-state drive current and OFF-state leakage current ratio (I_{ON}/I_{OFF}). For this concern, we have compared BP-JLFET-based biosensor and DM-TFET-based biosensor in terms of their I_{ON}/I_{OFF} ratio. From the observation, it is found that the DM-TFET-based biosensor has lower I_{ON}/I_{OFF} ratio in the order of $\sim 10^5$, whereas in BP-JLFET-based biosensor, the ratio of I_{ON}/I_{OFF} is in the order of $\sim 10^8$. The improvement in the drain sensitivity of BP-JLFET-based biosensor with an increased I_{ON}/I_{OFF} ratio makes it as the prominent device for the biosensing applications compared to DM-TFET-based biosensor. The sensitivity of BP-JLFET has also been compared with the conventional DM-FET-based biosensor to investigate the sensing capability of the proposed device.

III. Fabrication Flow of BP-JLFET-Based Biosensor

The process flow for the fabrication of BP-JLFET biosensor is shown in Fig. 3 [20]. The process begins with a lightly doped p-type silicon wafer, as shown in Fig. 3(a). On the silicon wafer, a uniformly doped n-type layer is formed by using arsenic implantation. For the implantation, the optimal implant energy is considered of ~20 keV with a dose of $\sim 10^{15}$–10^{16} cm^{-2}, as shown in Fig. 3(b). After this, high-k (HfO_2) gate oxide of thickness 7 nm is grown by using atomic layer deposition (ALD) or plasma-enhanced chemical vapor deposition (PECVD) as shown in Fig. 3(c) and followed by the etching out of gate oxide from the edges for the formation of source/drain region contact, which is shown Fig. 3(d). However, to propose a biosensor, a nanocavity is formed for detection of biomolecules. In this concern, the gate oxide is selectively etched out to form the nanocavity with the use of HfO_2 etchant [21], [22], as shown in Fig. 3(e). After this, a gate electrode is patterned with the metal having work function of 5.1 eV to create the final structure of BP-JLFET-based biosensor, as shown in Fig. 3(f).

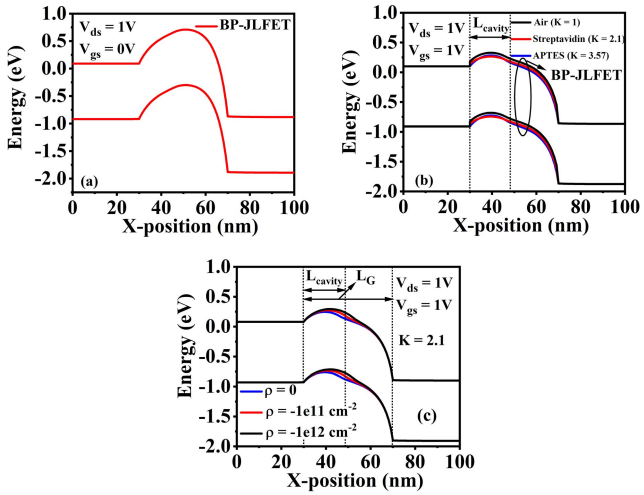

Fig. 4. Comparative plots of energy band diagram of BP-JLFET-based biosensor at (a) $V_{gs} = 0$ V and $V_{ds} = 1.0$ V, (b) different dielectric constant ($\rho = 0$) ($V_{gs} = 1.0$ V and $V_{ds} = 1.0$ V), and (c) different negative charge densities (K = 2) ($V_{gs} = 1.0$ V and $V_{ds} = 1.0$ V).

IV. Results and Discussion

A. Functionality of Neutral and Charged Biomolecules in the Cavity

In this section, the effect of neutral and charged biomolecules in the cavity has been investigated for all the three structures. In this concern, the energy band profile for the BP-JLFET-based biosensor at OFF- and ON-state along horizontal X-position for different dielectric constants (K) and charge densities (ρ) is shown in Fig. 4(a)–(c). Under the OFF state condition ($V_{gs} = 0$ V and $V_{ds} = 1$ V), it can be observed that there is no band bending for the movement of charge carriers between the valence band and the conduction band. However, at ON-state, the band profile bends at the junction near the source/channel interface with the immobilization of dielectric biomolecules in the formed cavity, and with an increase in the dielectric biomolecules value, the more bands bend at junction region, which enhances the coupling between the source and the channel, as shown in Fig. 4(b). From Fig. 4(c), it can be seen that with the increment in negative charge density, the coupling has been reduced due to increase in the barrier width of the energy band, which also changes the capacitive behavior at the junction. The electron density has been studied at different immobilizations of dielectric biomolecules underneath the gate dielectric to observe the changes in the behavior of Fermi potential of the device. Thus, from Fig. 5, it can be noticed that with an increase in dielectric constant of biomolecules, the energy density increases, leading to decrease in the Femi potential. The decrement in the Fermi potential bends the energy band toward the downward and increases the charge carriers movement through source/channel interface. Fig. 6(a) and (b) shows the transfer characteristics of BP-JLFET- and DM-TFET-based biosensor for different dielectric constants and negative charge densities, respectively. It is noticed from the figure that higher drain current of $\sim 10^{-6}$ A/μm at K = 3.57 has been achieved for BP-JLFET-based biosensor, and this has I_{ON}/I_{OFF} ratio of $\sim 10^8$, whereas, DM-TFET-based biosensor attains the drain

Authorized licensed use limited to: PRABIN KUMAR BERA. Downloaded on September 21,2022 at 13:31:50 UTC from IEEE Xplore. Restrictions apply.

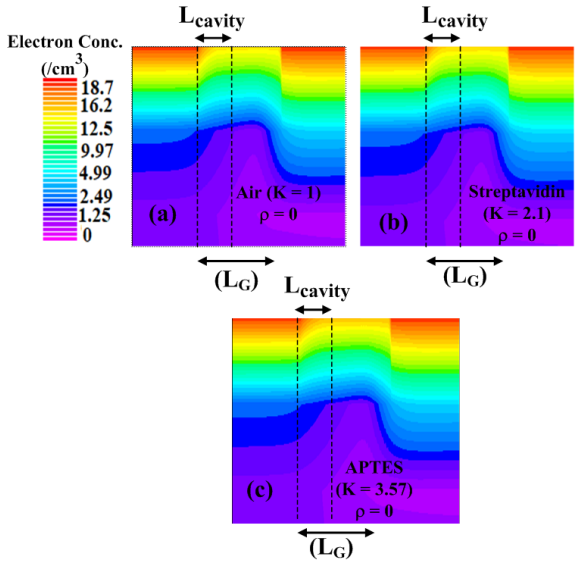

Fig. 5. (a)–(c) Contour plots of electron density variation for BP-JLFET-based biosensor at source/channel interface with the immobilization of a different dielectric constants ($\rho = 0$) in the nanocavity at $V_{gs} = 1.0$ V and $V_{ds} = 1.0$ V.

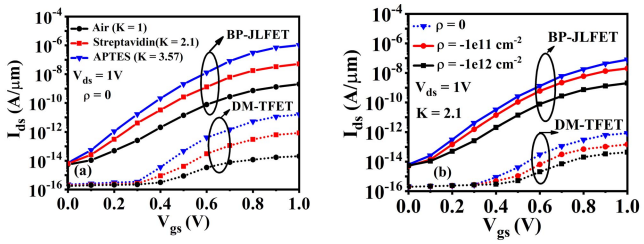

Fig. 6. Comparison of transfer characteristics for BP-JLFET- and DM-TFET-based biosensor at (a) different dielectric constants ($\rho = 0$) and (b) presence of negative charges in cm^{-2} (K = 2.1) at $V_{ds} = 1.0$ V.

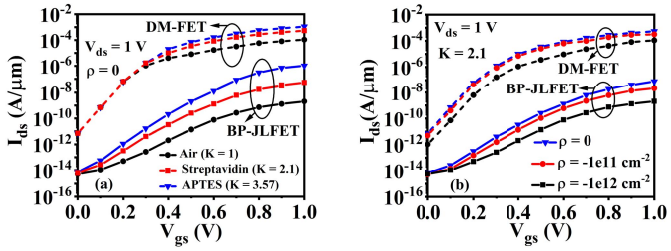

Fig. 7. Comparative plots of transfer characteristics for the conventional DM-FET- and BP-JLFET-based biosensor at different (a) dielectric constants ($\rho = 0$) and (b) negative charge densities (K = 2.1) at $V_{ds} = 1.0$ V.

current in the order of 10^{-11} A/μm at K = 3.57 and achieves I_{ON}/I_{OFF} ratio of $\sim 10^6$. The I_{ON}/I_{OFF} ratio is one of the parameters used to calculate the sensitivity of a device. In this concern, the BP-JLFET-based biosensor has better sensitivity in terms of I_{ON}/I_{OFF} ratio. The drain current along V_{gs} at fixed dielectric constant for different negative charge densities is shown in Fig. 6(b). From this figure, it can be depicted that drain current decreases with an increase in negative charge density that is due to a decrease in the effective gate potential, which results in low controlling of gate on the channel [shown in Fig. 4(c)].

In Fig. 7(a) and (b), the comparison between the conventional DM-FET- and proposed BP-JLFET-based biosensor has been shown in terms of transfer characteristics for different

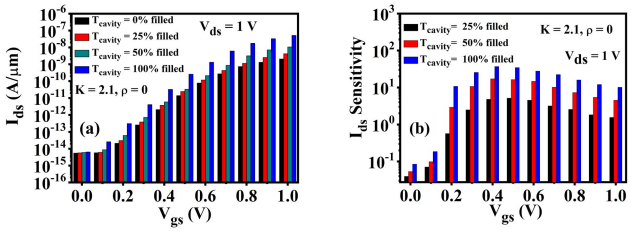

Fig. 8. (a) Plot of transfer characteristics of BP-JLFET-based biosensor with percentage volume variation in T_{cavity} filling from HfO_2/Si interface and (b) its sensitivity for K = 2.1 and $\rho = 0$ at $V_{ds} = 1.0$ V.

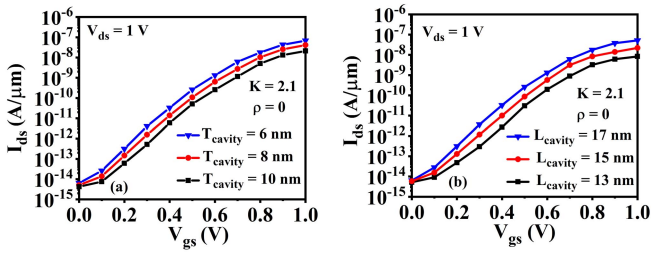

Fig. 9. Plots of transfer characteristics for BP-JLFET-based biosensor at different (a) thicknesses of cavity (T_{cavity}) and (b) lengths of cavity (L_{cavity}) at $V_{ds} = 1.0$ V.

dielectric constants and negative charge densities, respectively. From the figure, it can be noticed that the conventional DM-FET has higher drain current compared to the BP-JLFET-based biosensor. However, the change in drain current for the immobilization of different dielectric constant and the negative charge density in the cavity is higher in the proposed device, which consequently measures the sensitivity for the presence and absence of biomolecules. However, the sensitivity of a device is also directly dependent on the change in the geometrical size of the nanocavity [23]. The impact of percentage volume filling of the nanocavity to the downward direction for the BP-JLFET is shown in Fig. 8(a). The figure depicted that as the conjugation of the biomolecules decreases underneath the gate dielectric resulted toward the decrement in the drain current of the device. The decrement in drain current is due to nondegenerative carriers. In Fig. 8(b), the sensitivity is measured to see the performance of the proposed device with the different percentages of volume filling in the nanocavity. The effect with the change in geometrical parameters of the nanocavity on BP-JLFET-based biosensor has been studied in terms of transfer characteristics to evaluate the sensitivity of a device. Fig. 9(a) and (b) shows the transfer characteristics with change in thickness and length of the nanocavity at K = 2.1 ($\rho = 0$). As the thickness of the cavity increases, the barrier width between the source/channel interface increases that reduces the interaction between the two biomolecules, leading to decrease in the drain current, as shown in Fig. 9(a). With an increase in the length of the cavity, the movement of free charges from the valence band to conduction band increases, which results in the enhancement of drain current of a device, as shown in Fig. 9(b).

B. Analysis of Sensitivity for the Biosensors

It is essential to analyze the sensitivity of any biosensor to detect the presence of target biomolecules. The presence of

Authorized licensed use limited to: PRABIN KUMAR BERA. Downloaded on September 21,2022 at 13:31:50 UTC from IEEE Xplore. Restrictions apply.

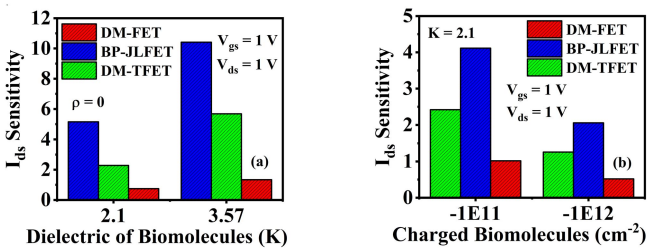

Fig. 10. Comparative plots of sensitivity for the conventional DM-FET-, BP-JLFET-, and DM-TFET-based biosensor at different (a) dielectric constants ($\rho = 0$), and (b) negative charge densities (K = 2.1) at $V_{gs} = 1.0$ V and $V_{ds} = 1.0$ V.

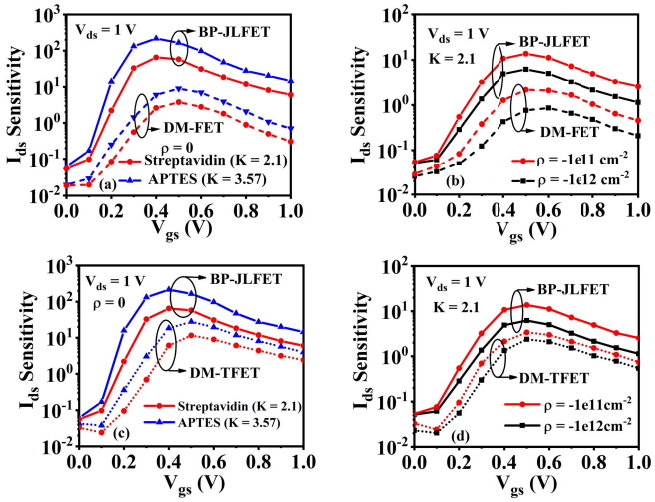

Fig. 11. Comparative plots of I_{ds} sensitivity along V_{gs} for the conventional DM-FET- and BP-JLFET-based biosensor at different (a) dielectric constants ($\rho = 0$), and (b) negative charge densities (K = 2.1) at $V_{ds} = 1.0$ V. Comparative plots of I_{ds} sensitivity along V_{gs} for the BP-JLFET- and DM-TFET-based biosensor at different (c) dielectric constants ($\rho = 0$) and (d) negative charge densities (K = 2.1) at $V_{ds} = 1.0$ V.

target in the cavity leads to a change in the drain current of the device, and this change in the parameter is used for the evaluation of the drain current sensitivity. For the calculation, the expression is defined as [2], [3], [24]

$$S_{\text{drain}} = \left(\frac{I^{\text{bio}}_{\text{drain}} - I^{air}_{drain}}{I^{\text{air}}_{\text{drain}}} \right) \tag{1}$$

where, in given expression (1), $I^{\text{bio}}_{\text{drain}}$ and $I^{\text{air}}_{\text{drain}}$ represent the ON-state drain current (calculated at $V_{gs} = 1$ V and $V_{ds} = 1$ V) in the presence and absence of the biomolecules (K = 1 (air)) in the nanocavity, respectively. This method of calculations of sensitivity has also been used by various researchers [2], [3], [24], [25]. Fig. 10(a) and (b) shows the drain current sensitivity plots at different dielectric constants (K) and charge densities ($\rho = 0$) for the conventional DM-FET-, BP-JLFET-, and DM-TFET-based biosensors, respectively. From the figure, it can be observed that the drain current sensitivity graph for K = 3.57 ($\rho = 0$) is higher than the other dielectric biomolecules present in the cavity due to having higher drain current [as shown in Figs. 6(a) and 7(a)]; as the drain current increases with an increase in dielectric constant (K), there is an increment in the drain current sensitivity of the device, which is shown in

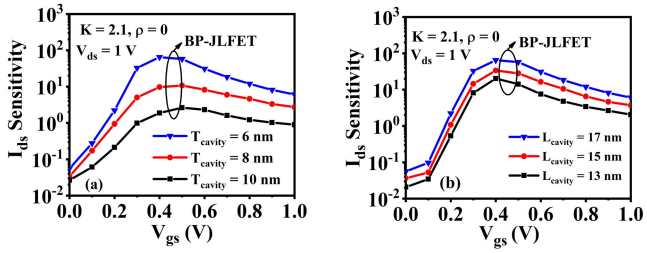

Fig. 12. Plots of I_{ds} sensitivity along V_{gs} for BP-JLFET-based biosensor at different (a) thicknesses of cavity (T_{cavity}) and (b) lengths of cavity (L_{cavity}) for streptavidin (K = 2.1 and $\rho = 0$) biomolecules at $V_{ds} = 1.0$ V.

Fig. 10(a). Similarly, the drain current sensitivity for different negative charge densities at fixed dielectric constant (K = 2.1) is shown in Fig. 10(b). It can be seen that the drain current sensitivity decreases with an increase in negative charge density. Thus, the dependence on drain current makes the changes in the drain current sensitivity, and the reduction in drain current with the higher value of negative charge density [as seen in Figs. 6(b) and 7(b)] leads to decrease in the drain current sensitivity of both the devices. However, from Fig. 10(a) and (b), it can also be noticed that the higher drain current sensitivity is achieved for the BP-JLFET-based biosensor in comparison to the conventional DM-FET- and DM-TFET-based biosensor at different dielectric constants and the negative charge densities, which reveals that the BP-JLFET-based biosensor has better capability for the detection of present biomolecules in the given solution. Furthermore, for the better comparison of the sensitivity, the conventional DM-FET-, BP-JLFET-, and DM-TFET-based biosensor are measured in terms of plotted graphs at the presence of different dielectric constants and the negative charge density in the cavity along V_{gs}, as shown in Fig. 11(a)–(d). From Fig. 11(a) and (b), it can be observed that the sensitivity for BP-JLFET-based biosensor is more pronounced at lower gate bias compared to the conventional DM-FET. This occurs due to higher change in drain current of BP-JLFET-based biosensor [can be seen from Fig. 7(a) and (b)] and that turns into higher sensitivity for the better detection of the biomolecules. Similarly, from Fig. 11(c) and (d), it can be depicted that the sensitivity for the BP-JLFET is higher than that for DM-TFET-based biosensor at different dielectric constants and negative charge densities at moderate gate voltage bias. Furthermore, the variation in drain sensitivity for the change in the geometrical parameters of the nanocavity is also shown in Fig. 12(a) and (b) for the immobilization of streptavidin (K = 2.1). Thus, with an increase in the thickness of the gate oxide, there is a decrease in generation and recombination rate of the carriers that resulted in the reduction of the overall drain current. In that aspect, as the thickness of the nanocavity increases, the reduction in the generation rate of carriers occurs, which leads to a decrease in drain current that in turn decreases the sensitivity of the device, as shown in Fig. 12(a). In a similar manner, with decrease in length of the cavity, the sensitivity decreases, because as with shortening of the nanocavity length, the carriers get closely associated with each other, and this affects the generation process, which results in decrease in the sensitivity, as noticed from Fig. 12(b).

Authorized licensed use limited to: PRABIN KUMAR BERA. Downloaded on September 21,2022 at 13:31:50 UTC from IEEE Xplore. Restrictions apply.

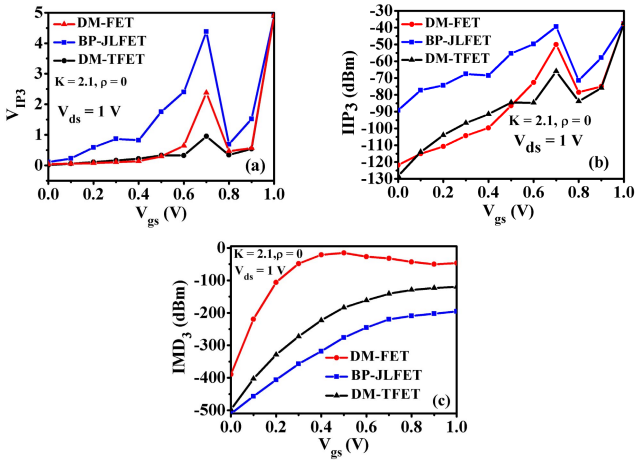

Fig. 13. Comparative plots of (a) V_{IP3}, (b) IIP_3, and (c) IMD_3 along V_{gs} for the conventional DM-FET-, BP-JLFET-, and DM-TFET-based biosensors at $V_{ds} = 1.0$ V.

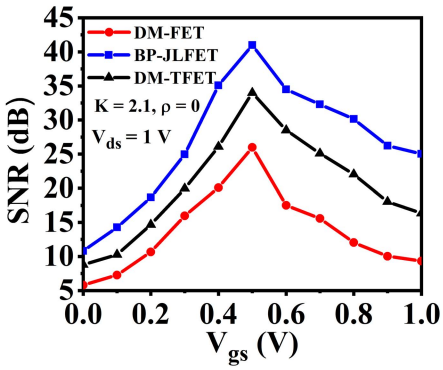

Fig. 14. Comparative plots of signal-to-noise ratio (SNR) along V_{gs} for the conventional DM-FET-, BP-JLFET-, and DM-TFET-based biosensors at $V_{ds} = 1.0$ V.

C. Noise Analysis of Field-Effect Transistor-Based Biosensors

The researchers have been suggested that the linearity and the noise are somehow correlated with each other [25], [26]. Therefore, to analyze the performance of the proposed device in the presence of noise, we measured the noise characteristics of all the three structures with the consideration of the linearity parameters that are V_{IP3}, third-order input intercept point (IIP_3), and third-order intermodulation (IMD_3), as shown in Fig. 13(a)–(c). V_{IP3} defines the extrapolated input voltage in which the first- and the third-harmonic voltages are the same, and this V_{IP3} should be high to reduce the impact of noise of a device. From Fig. 13(a), it can be noticed that V_{IP3} for the proposed device along V_{gs} shows the higher point of value in comparison to both the simulated devices. The peak value of V_{IP3} defines the third-order nonlinearity factor cancellation by the internal feedback device throughout the second-order nonlinearity [27]. The less distortion and better signal-to-noise ratio (SNR) required for the better sensitivity of the biosensor, which is observed from Fig. 13(b). The shown figure inferred that the lower distortion of the proposed structure with the higher IIP_3 value has the better sensitivity. The IMD_3 describes the harmonic distortion of the structures with the factor of intermodulation current. For the better performance of the biosensor in the presence of noise, the IMD_3 value should be low. It can be noticed from Fig. 13(c) that the proposed device has the lower IMD_3 value. The evaluated parameters imply that the BP-JLFET-based biosensor is less affected under noise conditions compared to the conventional DM-FET and DM-TFET biosensor due to more maintaining the linearity system of the device with the improved linearity parameters of the proposed device. The performance of SNR also enhances with the better linearity due to interdependency, which results in the better sensing capability of the proposed device.

D. SNR Analysis of Field-Effect Transistor-Based Biosensors

The sensitivity and selectivity are the most important parameters to detect the specific presence of biomolecules on the surface of receptors of the biosensors. The FET-based biosensors with better sensitivity and the selectivity are useful in-point of care systems to diagnose the disease by selecting the right cells among the presence of various cells in the human body, while in the detection of specific biomolecules to diagnose the disease, various parasitic biomolecules (air) sit on the surface of receptor. Since the size of the biomolecules differs and could not cover the whole surface area of the nanocavity, for the detection of target biomolecules in the presence of parasitic biomolecules on the surface, this behaves like the noise. In the FET-based biosensor, the channel noise or disturbances are more prominent [28] due to the modification of dielectric at the source/channel interface. Therefore, to address this issue, we have measured and compared the SNR of the conventional DM-FET and DM-TFET with the proposed BP-JLFET-based biosensor (see Fig. 14). For the calculation of SNR value, the expression is given as [29]

$$\mathrm{SNR(dB)} = 20\log_{10}\left(\frac{|\,\mu_{\mathrm{true}} - \mu_{\mathrm{false}}\,|}{2\sigma}\right). \tag{2}$$

In expression (2), μ_{true} and μ_{false} define the mean true (target biomolecule) value and mean false (parasitic biomolecule) value for the signal amplitude, respectively, whereas σ is the mean standard deviation for true and false value of the noise amplitude. It has also been shown that the SNR value is interrelated with the intermodulation distortion (IMD_3) [31]. From Fig. 13(c), it can be noticed that the conventional DM-FET and DM-TFET have more distortion in the signal. Thus, from here, it can be observed that the conventional DM-FET and the DM-TFET have low SNR value, which includes more noise factor and has a low tendency to detect the specific presence of biomolecules in the presence of multiple biomolecules on the receptor surface. From Fig. 14, it can be clearly seen that in comparison to the conventional DM-FET and the DM-TFET, the proposed BP-JLFET-based biosensor has a higher SNR value. Furthermore, the SNR peak value for the BP-JLFET is ∼42 dB, whereas the conventional DM-FET and the DM-TFET are ∼25 and ∼35 dB, respectively, which depicts the presence of low noise factor in the proposed BP-JLFET-based biosensor. Thus, the higher SNR peak value increases the selectivity, which plays an important role to

Authorized licensed use limited to: PRABIN KUMAR BERA. Downloaded on September 21,2022 at 13:31:50 UTC from IEEE Xplore. Restrictions apply.

design the impactful biosensor for the detection of specific biomolecules in the presence of parasitic biomolecules [32].

V. Conclusion

In this article, an ultrathin BP-JLFET-based biosensor has been investigated for the detection of neutral and charged biomolecules in the etched nanocavity underneath the gate dielectric. It has been observed that, with the immobilization of APTES (K = 3.57) on the surface, the measured sensitivity for BP-JLFET-based biosensor is ∼20% and 10% higher than that for the conventional DM-FET- and DM-TFET-based biosensor, respectively. Moreover, in case of streptavidin (K = 2.1), the sensitivity for BP-JLTFET is 16% and 8% higher than that for the conventional DM-FET- and DM-TFET-based biosensor, respectively. It has also been observed that the proposed BP-JLFET-based biosensor is ∼50% less affected in comparison to the conventional DM-FET- and DM-TFET-based biosensor under noise conditions. Furthermore, in comparison with the conventional DM-FET and DM-TFET, the proposed BP-JLFET-based biosensor has a higher SNR peak value of 42 dB for the streptavidin (K = 2.1) biomolecules with the low limit of detection (LOD) of 0.1, which signifies the higher selectivity of the biomolecules to diagnose the disease in the presence of multiple biomolecules in human being.

References

[1] P. Bergveld, "Development, operation, and application of the ion-sensitive field-effect transistor as a tool for electrophysiology," *IEEE Trans. Biomed. Eng.*, vol. BME-19, no. 5, pp. 342–351, Sep. 1972, doi: 10.1109/TBME.1972.324137.

[2] D. Singh, S. Pandey, K. Nigam, D. Sharma, D. S. Yadav, and P. Kondekar, "A charge-plasma-based dielectric-modulated junctionless TFET for biosensor label-free detection," *IEEE Trans. Electron Devices*, vol. 64, no. 1, pp. 271–278, Jan. 2017, doi: 10.1109/TED.2016.2622403.

[3] S. A. Hafiz, Iltesha, M. Ehteshamuddin, and S. A. Loan, "Dielectrically modulated source-engineered charge-plasma-based Schottky-FET as a label-free biosensor," *IEEE Trans. Electron Devices*, vol. 66, no. 4, pp. 1905–1910, Apr. 2019, doi: 10.1109/TED.2019.2896695.

[4] C.-A. Vu and W.-Y. Chen, "Field-effect transistor biosensors for biomedical applications: Recent advances and future prospects," *Sensors*, vol. 19, no. 19, p. 4214, Sep. 2019, doi: 10.3390/s19194214.

[5] S. Kim, D. Baek, J.-Y. Kim, S.-J. Choi, M.-L. Seol, and Y.-K. Choi, "A transistor-based biosensor for the extraction of physical properties from biomolecules," *Appl. Phys. Lett.*, vol. 101, no. 7, Aug. 2012, Art. no. 073703, doi: 10.1063/1.4745769.

[6] H. Im, X.-J. Huang, B. Gu, and Y.-K. Choi, "A dielectric-modulated field-effect transistor for biosensing," *Nature Nanotechnol.*, vol. 2, no. 7, pp. 430–434, Jul. 2007, doi: 10.1038/nnano.2007.180.

[7] X. Chen *et al.*, "Electrical nanogap devices for biosensing," *Mater. Today*, vol. 13, no. 11, pp. 28–41, Nov. 2010, doi: 10.1016/S1369-7021(10)70201-7.

[8] J.-M. Choi, J.-W. Han, S.-J. Choi, and Y.-K. Choi, "Analytical modeling of a nanogap-embedded FET for application as a biosensor," *IEEE Trans. Electron Devices*, vol. 57, no. 12, pp. 3477–3484, Dec. 2010, doi: 10.1109/TED.2010.2076152.

[9] A. Matsumoto and Y. Miyahara, "Current and emerging challenges of effeld effect transistor based biosensing," *Nanoscale*, vol. 5, no. 22, pp. 10702–10718, Sep. 2013, doi: 10.1039/C3NR02703A.

[10] D. Sarkar and K. Banerjee, "Fundamental limitations of conventional-FET biosensors: Quantum-mechanical-tunneling to the rescue," in *Proc. 70th Device Res. Conf.*, Jun. 2012, pp. 83–84, doi: 10.1109/DRC.2012.6256950.

[11] D. Shafizade, M. Shalchian, and F. Jazaeri, "Ultrathin junctionless nanowire FET model, including 2-D quantum confinements," *IEEE Trans. Electron Devices*, vol. 66, no. 9, pp. 4101–4106, Sep. 2019, doi: 10.1109/TED.2019.2930533.

[12] J. Hur *et al.*, "A core compact model for multiple-gate junctionless FETs," *IEEE Trans. Electron Devices*, vol. 62, no. 7, pp. 2285–2291, Jul. 2015, doi: 10.1109/TED.2015.2428711.

[13] M.-S. Yeh, Y.-C. Wu, M.-H. Wu, M.-H. Chung, Y.-R. Jhan, and M.-F. Hung, "Characterizing the electrical properties of a novel junctionless poly-Si ultrathin-body field-effect transistor using a trench structure," *IEEE Electron Device Lett.*, vol. 36, no. 2, pp. 150–152, Feb. 2015, doi: 10.1109/LED.2014.2378785.

[14] S. Gundapaneni, S. Ganguly, and A. Kottantharayil, "Bulk planar junctionless transistor (BPJLT): An attractive device alternative for scaling," *IEEE Electron Device Lett.*, vol. 32, no. 3, pp. 261–263, Mar. 2011, doi: 10.1109/LED.2010.2099204.

[15] S. Gundapaneni, M. Bajaj, R. K. Pandey, K. V. R. M. Murali, S. Ganguly, and A. Kottantharayil, "Effect of band-to-band tunneling on junctionless transistors," *IEEE Trans. Electron Devices*, vol. 59, no. 4, pp. 1023–1029, Apr. 2012, doi: 10.1109/TED.2012.2185800.

[16] R. Narang, M. Saxena, and M. Gupta, "Modeling and simulation investigation of sensitivity of symmetric split gate junctionless FET for biosensing application," *IEEE Sensors J.*, vol. 17, no. 15, pp. 4853–4861, Aug. 2017, doi: 10.1109/JSEN.2017.2716102.

[17] M. S. Parihar and A. Kranti, "Enhanced sensitivity of double gate junctionless transistor architecture for biosensing applications," *Nanotechnology*, vol. 26, no. 14, Apr. 2015, Art. no. 145201, doi: 10.1088/0957-4484/26/14/145201.

[18] S. Kalra, M. J. Kumar, and A. Dhawan, "Dielectric-modulated field effect transistors for DNA detection: Impact of DNA orientation," *IEEE Electron Device Lett.*, vol. 37, no. 11, pp. 1448–1485, Sep. 2016, doi: 10.1109/LED.2016.2613110.

[19] C. H. Kim, C. Jung, K. B. Lee, H. G. Park, and Y. K. Choi, "Label-free DNA detection with a nanogap embedded complementary metal oxide semiconductor," *Nanotechnology*, vol. 22, no. 13, pp. 1–5, Apr. 2011, doi: 10.1088/0957-4484/22/13/135502.

[20] R. Garike and G. C. Patil, "Si_3N_4: HfO_2 dual-k spacer bulk planar junctionless transistor for mixed signal integrated circuits," *IET Circuits, Devices Syst.*, vol. 13, no. 1, pp. 45–50, Jan. 2019, doi: 10.1049/iet-cds.2018.5168.

[21] J. Starzynski, "Selective hafnium oxide etchant," U.S. Patent 10 938 191, Mar. 16, 2006.

[22] D. Shamiryan, V. Paraschiv, and M. Demand, "Plasma composition for selective high-k etch," U.S. Patent 7 598 184, Oct. 6, 2009.

[23] J.-H. Ahn, S.-J. Choi, J.-W. Han, T. J. Park, S. Y. Lee, and Y.-K. Choi, "Investigation of size dependence on sensitivity for nanowire FET biosensors," *IEEE Trans. Nanotechnol.*, vol. 10, no. 6, pp. 1405–1411, Nov. 2011, doi: 10.1109/TNANO.2011.2157519.

[24] D. Singh and G. C. Patil, "Performance analysis of feedback field-effect transistor-based biosensor," *IEEE Sensors J.*, vol. 20, no. 22, pp. 13269–13276, Nov. 2020, doi: 10.1109/JSEN.2020.3006986.

[25] M. Verma, S. Tirkey, S. Yadav, D. Sharma, and D. S. Yadav, "Performance assessment of a novel vertical dielectrically modulated TFET-based biosensor," *IEEE Trans. Electron Devices*, vol. 64, no. 9, pp. 3841–3848, Sep. 2017, doi: 10.1109/TED.2017.2732820.

[26] B. Razavi, *Design of Analog CMOS Integrated Circuits*, vol. 677. New York, NY, USA: McGraw-Hill, 2000.

[27] P. Ghosh, S. Haldar, R. S. Gupta, and M. Gupta, "An investigation of linearity performance and intermodulation distortion of GME CGT MOSFET for RFIC design," *IEEE Trans. Electron Devices*, vol. 59, no. 12, pp. 3263–3268, Dec. 2012, doi: 10.1109/TED.2012.2219537.

[28] N. K. Rajan, K. Brower, X. Duan, and M. A. Reed, "Limit of detection of field effect transistor biosensors: Effects of surface modification and size dependence," *Appl. Phys. Lett.*, vol. 104, no. 8, Feb. 2014, Art. no. 084106, doi: 10.1063/1.4867025.

[29] J. Beal, "Signal-to-noise ratio measures efficacy of biological computing devices and circuits," *Frontiers Bioeng. Biotechnol.*, vol. 3, p. 93, Jun. 2015, doi: 10.3389/fbioe.2015.000937.

[30] B. Jin *et al.*, "Electrical characteristics and pH response of a parylene-H sensing membrane in a Si-nanonet ion-sensitive field-effect transistor," *Sensors*, vol. 18, no. 11, p. 3892, Nov. 2018, doi: 10.3390/s18113892.

[31] V. A. Abramsky, K. Balachandran, K. K. Chang, and K. M. Rege, "Combined RSSI/SNR-driven intermodulation-mitigation scheme for CDMA terminals," U.S. Patent 6 052 566, Apr. 18, 2000.

[32] S. Nishitani and T. Sakata, "Enhancement of signal-to-noise ratio for serotonin detection with well-designed nanofilter-coated potentiometric electrochemical biosensor," *ACS Appl. Mater. Interface*, vol. 12, no. 13, pp. 14761–14769, Mar. 2020, doi: 10.1021/acsami.9b19309.

Authorized licensed use limited to: PRABIN KUMAR BERA. Downloaded on September 21,2022 at 13:31:50 UTC from IEEE Xplore. Restrictions apply.